LOCALISATION OF FLOW-INDUCED NOISE SOURCE GENERATED AT THE AEOLIAN TONE USING HYBRID CFD-BEM AND TIME-REVERSAL METHOD

Paul Croaker[1], Akhilesh Mimani[2], Con J. Doolan[1] and Nicole Kessissoglou[1]

[1]School of Mechanical and Manufacturing Engineering
UNSW Australia, Sydney NSW 2052, Australia
Email: p.croaker@unsw.edu.au
c.doolan@unsw.edu.au
n.kessissoglou@unsw.edu.au

[2]School of Mechanical Engineering,
The University of Adelaide, Adelaide SA 5005, Australia
Email: akhilesh.mimani@adelaide.edu.au

Abstract

This paper presents a novel simulation technique based on the hybrid computational fluid dynamics (CFD)-boundary-element method (BEM) and the aeroacoustic Time-Reversal (TR) source localisation method to analyse the flow-induced noise generated at the Aeolian tone due to a circular cylinder located in a low Mach number flow. To this end, the hybrid CFD-BEM method is used to obtain the far-field acoustic spectrum of (1) the direct acoustic pressure field generated by flow over the cylinder, (2) the acoustic field scattered by the cylinder and (3) the total acoustic field at all four computational boundaries. The acoustic spectrum shows the occurrence of an Aeolian tone for all three cases whereby the acoustic pressure time-history at the boundary nodes is synthesised by assuming a sinusoidal signal at the Aeolian tone frequency. The aeroacoustic TR simulation was implemented by numerically solving a set of 2-D Linearised Euler Equations (LEE) and enforcing the time-reversed acoustic pressure history as input at the computational boundaries. The TR source maps indicate a lateral quadrupole source nature due to the direct field whilst a lift-dipole source nature is indicated due to the scattered and total acoustic pressure fields. The results of the TR simulations is consistent with previous works, thereby demonstrating the validity of the novel technique proposed in this work for analysing flow-induced noise problems.

1. Introduction

This paper investigates the problem of localisation of aeroacoustic noise sources produced by turbulent flow over a circular cylinder at the Aeolian tonal frequency. This problem has been well studied in the literature by combining experimental acoustic pressure measurements with source localisation techniques such as Conventional Beamforming (CB), see Ref. [1] as well as the aeroacoustic Time-Reversal (TR) simulation, see Ref. [2]. These studies have demonstrated that at the vortex-shedding or the Aeolian tone frequency, localisation of aeroacoustic sources from far-field acoustic pressure measurements yields a lift-dipole source that is located near the cylinder-axis [3]. The novelty of the present work is to combine for the first time, a hybrid CFD-BEM technique [4] with the aeroacoustic TR source localisation technique for characterising the flow-induced noise sources. The combined approach is demonstrated on the benchmark problem of flow over a circular cylinder. The hybrid

CFD-BEM technique is used to obtain the simulated far-field acoustic pressure data at the Aeolian tonal frequency over a line array of nodes. This numerical acoustic data is then used as input Dirichlet boundary conditions during aeroacoustic TR simulation to characterise the flow-induced Aeolian tone source. The main advantage of numerically computing the far-field sound pressure is that it can be decomposed into direct and scattered components which can also yield the total far-field acoustic pressure. The TR method is then implemented using individual far-field acoustic pressure components (direct, scattered and total) to investigate their respective source characteristics.

The paper is organised as follows. Section 2 describes the methodology for implementing the hybrid CFD-BEM technique and also presents the results showing the hydrodynamic and flow-induced acoustic far-field for turbulent flow over a circular cylinder at a Reynolds number Re_D=46,000 (based on the cylinder diameter) and a Mach number M=0.21. Section 3 describes the technique for synthesising the acoustic pressure time-history at the computational boundaries for use during the TR simulations from the far-field spectral data of the flow-induced noise of a cylinder obtained using hybrid CFD-BEM method. Section 4 briefly describes the methodology for implementing TR simulations using a high-resolution computational aeroacoustics algorithm. Section 5 analyses the TR source maps due to the direct, scattered and total acoustic pressure fields. Section 6 presents a summary of this work.

2. Hybrid CFD-BEM: Methodology and Results

A hybrid CFD-BEM technique is used to predict the flow-induced noise generated by turbulent flow past a circular cylinder. This technique involves the following steps:

1. A CFD analysis using Large Eddy Simulation (LES) is used to predict the unsteady turbulent flow-field around the cylinder and to extract the flow-induced noise sources based on the Lighthill's acoustic analogy [5];
2. The propagation of the acoustic waves generated by the flow-induced noise sources and prediction of the near-field pressure and pressure gradient incident on the cylinder surface;
3. Application of the incident field to a BEM model of the cylinder based on the Burton-Miller formulation [6] and calculation of the resulting far-field acoustic pressure. The far-field acoustic pressure is recorded at the data recovery nodes corresponding to the boundary nodes of the TR mesh.

2.1 Hydrodynamic simulation

Turbulent flow over a circular cylinder of diameter D=10 mm was simulated at a Reynolds number Re_D=46,000 (based on the diameter) at a free-stream velocity $U_\infty = 72\ \mathrm{m \cdot s^{-1}}$ or Mach number M=0.21. A three-dimensional circular domain around the cylinder was modelled and analysed using OpenFOAM [7]. The turbulent flow-field is simulated by incompressible LES, which solves the filtered incompressible Navier-Stokes equations. The LES equations were solved using an iterative, segregated solution method with the pressure-velocity coupling handled using the Pressure Implicit with Splitting of Operator (PISO) algorithm.

The interior of the computational domain used for the LES simulation extends radially for 30D. A sponge layer extends radially for an additional 30D. The interior domain contains 2.28 million hexahedral cells, with a cell spacing adjacent to the cylinder of $1.3\times10^{-3}D$. The sponge-layer contains an additional 180,000 hexahedral cells. The cells in the sponge-layer grow rapidly in the radial direction to damp out fluctuations in the velocity field and suppress generation of acoustic waves caused by vorticity leaving the domain. The transient simulation was allowed to progress until the flow-field achieved quasi-periodicity beyond which the time-history of the acoustic source data was recorded using two equal Welch segments and converted into the frequency-domain.

2.2 Near-field formulation for the flow-induced noise propagation

The propagation of the acoustic waves generated by the flow-induced noise sources to the surface of the cylinder is resolved using formulations for the near-field pressure and pressure gradient derived based on Lighthill's analogy [4]. The incident pressure p_a^i and its normal derivative $q_{a,\,n}^i$ on the body are given by

$$p_a^i(\mathbf{x},\,\omega)=\lim\nolimits_{\in\to 0}\int_{(\Omega-V_\in)} T_{ij}(\mathbf{y},\,\omega)\frac{\partial^2 G_h}{\partial y_i \partial y_j}\mathrm{d}y \tag{1}$$

$$q_{a,\,n}^i(\mathbf{x},\,\omega)=\lim\nolimits_{\in\to 0}\int_{(\Omega-V_\in)} T_{ij}(\mathbf{y},\,\omega)\frac{\partial^3 G_h}{\partial y_i \partial y_j \partial n}\mathrm{d}y \tag{2}$$

where y_i is the i^{th} component of the acoustic source point position vector **y**. It is noted that **x** is the field point where the near-field pressure and its normal derivative are recovered, Ω is the computational domain and $V_\in$ represents an exclusion neighbourhood taken around the field point. This exclusion neighbourhood allows the singularities occurring when **y**=**x** to be regularised. The harmonic free-field Green's function of the wave equation is given by

$$G_h=\frac{\mathrm{e}^{\mathrm{j}k_a r}}{4\pi r} \tag{3}$$

where $\mathrm{j}=\sqrt{-1}$, the imaginary unit, k_a is the acoustic wavenumber and $r=|\mathbf{x}-\mathbf{y}|$. Furthermore, T_{ij} is the Lighthill tensor [5] represented by $T_{ij}=\rho_0 u_i u_j$, where u_i is the i^{th} component of the velocity vector and $\rho_0=1.21\,\mathrm{kg\cdot m^{-3}}$ is the density of the fluid. Additional details of the formulations for the near-field pressure and pressure gradient as well as their numerical treatment can be found in Ref. [4].

2.3 Scattering of the incident aeroacoustic fields using BEM

The inhomogeneous Helmholtz equation is given by

$$\Delta p_a(x)+k_a^2 p_a=-Q \tag{4}$$

where the inhomogeneity Q is an acoustic source. Applying the method of Burton and Miller [6] to Eq. (4) and combining with the incident field produced by the aeroacoustic sources yields

$$\begin{aligned}&c(\mathbf{y})p_a(\mathbf{y})+\int_\Gamma p_a(\mathbf{x})\frac{\partial G_h}{\partial n(\mathbf{x})}\mathrm{d}\Gamma+\mathrm{j}\beta\int_\Gamma p_a(\mathbf{x})\frac{\partial^2 G_h}{\partial n(\mathbf{x})\partial n(\mathbf{y})}\mathrm{d}\Gamma=\\ &\mathrm{j}\rho_0 c_0 k_a\left(\int_\Gamma \left(v_a(\mathbf{x})G_h\right)\mathrm{d}\Gamma-\mathrm{j}\beta\left(c(\mathbf{y})v_a(\mathbf{y})-\int_\Gamma v_a(\mathbf{x})\frac{\partial G_h}{\partial n(\mathbf{y})}\mathrm{d}\Gamma\right)\right)+p_a^i(\mathbf{y})+\mathrm{j}\beta q_a^i(\mathbf{y})\end{aligned} \tag{5}$$

where $c(\mathbf{y})$ is a free-term coefficient and equals 1 in the interior domain and 0.5 on a smooth boundary. Furthermore, n is the unit normal to the boundary, β is the Burton and Miller coupling parameter, $c_0=343\,\mathrm{m\cdot s^{-1}}$ is the sound speed of the fluid medium at rest and v_a is the fluid particle velocity. In this paper, Eq. (5) is solved using the two dimensional AEBEM2 solver of Kirkup [8]. The cylinder is discretised into 100 evenly spaced one-dimensional boundary elements.

2.4 Hydrodynamic results

The flow over the cylinder is in the sub-critical regime at a Reynolds number Re_D=46,000 and a Mach number M=0.21. Figure 1(a) shows an iso-surface of the normalised Q-criterion, with $Q_n=0.5Q\,D^2/U_\infty^2$, revealing turbulent structures in the flow. Figure 1(b) shows the non-dimensional span-wise vorticity γ^+ given by $\gamma^+=\gamma D/U_\infty$ on a plane passing through the centre of the cylinder's span. It is noted that γ denotes the vorticity. Figure 1 reveals that a shear-layer forms as the fluid separates from the cylinder. This shear layer becomes unstable and breaks up into small scale turbulent structures which develop and grow as they travel downstream. In the near-wake region large flow structures associated with the coherent vortex shedding are evident.

Table 1 compares the aerodynamic coefficients obtained by the present LES with numerical results [9] and experimental measurements [10] from the literature. The Strouhal number S_t predicted here is approximately 14% larger than the reference values. The time-averaged drag-coefficient $C_{D,\mathrm{av}}$ compares well with the numerical results of Seo and Moon [9], however, the rms values of the drag-coefficient $C_{D,\mathrm{rms}}$ are lower than the reference values. The rms value of the lift-coefficient, $C_{L,\mathrm{rms}}$ compares favourably with the experimental measurements of Szepessy and Bearman [10].

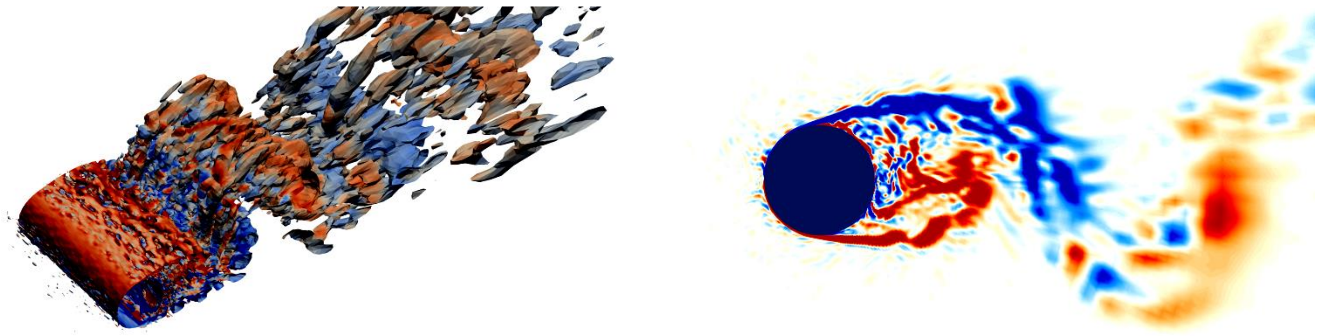

(a) Normalised $Q-$criteria, Q_n (b) Normalised vorticity, γ^+

Figure 1. Turbulent flow structures in the cylinder near-wake

Table 1. Comparison of the Strouhal number S_t, time-averaged drag-coefficient $C_{D,\mathrm{av}}$, rms drag-coefficient $C_{D,\mathrm{rms}}$ and RMS lift-coefficient $C_{L,\mathrm{rms}}$

	S_t	$C_{D,\mathrm{av}}$	$C_{D,\mathrm{rms}}$	$C_{L,\mathrm{rms}}$
Ref. [9]	0.187	1.24	0.1	0.54
Ref. [10]	0.19	1.35	0.16	0.45-0.5
Present work	0.216	1.21	0.074	0.49

2.5 Scattered acoustic pressure field

The incident field was computed using the near-field formulations for the pressure and pressure gradient given by Eqs. (1) and (2). The scattered fields were obtained using the AEBEM2 subroutine of Kirkup [8], solving the Burton and Miller formulation. AEBEM2 is a two-dimensional solver and the far-field pressure is converted from two dimensions to three dimensions and corrected for finite span using the long span technique of Seo and Moon [9].

Figure 2 shows the sound pressure level (SPL) for the entire span at a point directly above the mid-span of the cylinder and distance r=185D from the cylinder-axis.

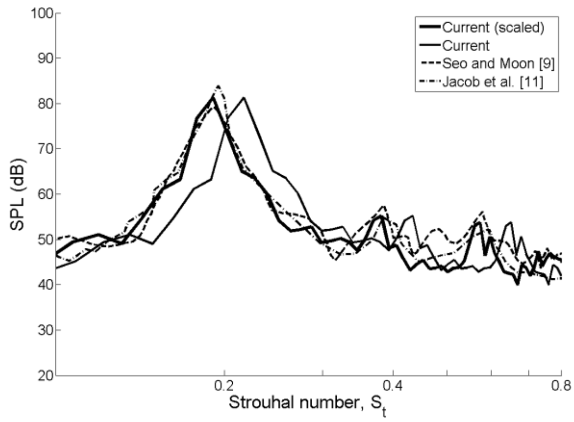

Figure 2. Sound pressure level (SPL) spectrum at distance r=185D from the mid-span of the cylinder

It is observed from Fig. 2 that the SPL predicted by the present method is in a good agreement with the numerical results of Seo and Moon [9] as well as with the experimental measurements obtained by Jacob *et al*. [11]. In particular, the peak SPL associated with the vortex-shedding is accurately captured with the hybrid CFD-BEM technique used here, thereby demonstrating its validity. In order to make a direct comparison easier, the frequency range of the present results is scaled so that the vortex-shedding frequency matches more closely with the results from Refs. 9 and 11.

2.6 Far-field acoustic pressure for source localisation

To localise the flow-induced noise sources, the far-field acoustic pressure was calculated on a square boundary of side length 70*D* centered on the cylinder. On each side of the square boundary, 200 evenly spaced data recovery points were positioned. The direct acoustic radiation from the flow-induced noise sources as well as the scattered and the total acoustic pressure fields were computed at these 800 data recovery points. The complex acoustic pressure boundary data (in the frequency domain) was converted into the time domain at these data recovery points which were then used as the input at the computational boundaries during TR simulation to characterise the flow-induced noise sources responsible for the direct, scattered and total far-field acoustic pressure fields.

3. Synthesising Acoustic Pressure Time-History from the Far-Field Spectrum

A simple method of synthesising the acoustic pressure time-history at the boundary nodes from the far-field spectral data of the flow-induced noise of a cylinder, obtained numerically using the hybrid CFD-BEM technique, is described. Figures 3(a)-(c) show the far-field spectrum of the direct, scattered and the total acoustic pressure field, respectively, at the node $x = -\ 0.177\ \mathrm{m}, y = -\ 0.35\ \mathrm{m}$ located on the bottom boundary. It is noted that the Strouhal number represents the non-dimensional frequency and is given by $S_t = fD/U_0$ where f, $D = 10\ \mathrm{mm}$ and $U_\infty = 72\ \mathrm{m{\cdot}s^{-1}}$ denote the frequency, cylinder diameter and free-stream velocity, respectively.

It is observed that Figs. 3(a)-(c) exhibit an Aeolian tone at $S_t \approx 0.21$ or equivalently at $f = 1562.5\ \mathrm{Hz},$ that is a characteristic feature of the flow-induced noise of a full-span cylinder [3, 12]. Since the focus of this work is to demonstrate the validity of the hybrid CFD-BEM and TR methods to analyse flow-induced noise at the Aeolian tone, the acoustic pressure at the boundary nodes is assumed to be a pure sinusoid of frequency equal to the Aeolian tone. Mathematically, $\tilde{p}(x_0, y_0, t) = A_0 \sin(2\pi f_a t + \phi_0),$ where $f_a = 1562.5\ \mathrm{Hz}$ denotes the Aeolian tonal frequency, A_0 and ϕ_0 are the amplitude and phase, respectively, of the sinusoidal signal at a given boundary node $(x_0,\ y_0)$ and *t* denotes the forward time. It is noted that the amplitude A_0 is obtained from the acoustic spectrum shown in Fig. 3 whilst the phase ϕ_0 is obtained from the real $\mathrm{Re}\{A_0\}$ and imaginary $\mathrm{Im}\{A_0\}$ parts that is known from the numerical CFD-BEM data. In order to ensure stability and a high accuracy of the TR simulations, a small value of the Courant–Friedrichs–Lewy (CFL) number [13] taken equal to 0.2 is considered, implying a time-step $\Delta t = 2.0417 \times 10^{-6}\mathrm{s}.$ In this work, a square domain of half-length $L_0 = 0.35\ \mathrm{m}$ is considered and each side is subdivided into 200 equal parts (201 nodes); therefore, the acoustic pressure time-history is synthesised at a total of 800 boundary nodes for a total of $N_{\max} = 10000$ time-steps. The synthesised time-history data which takes into account an accurate estimate of the amplitude and phase at each node is used during TR simulations.

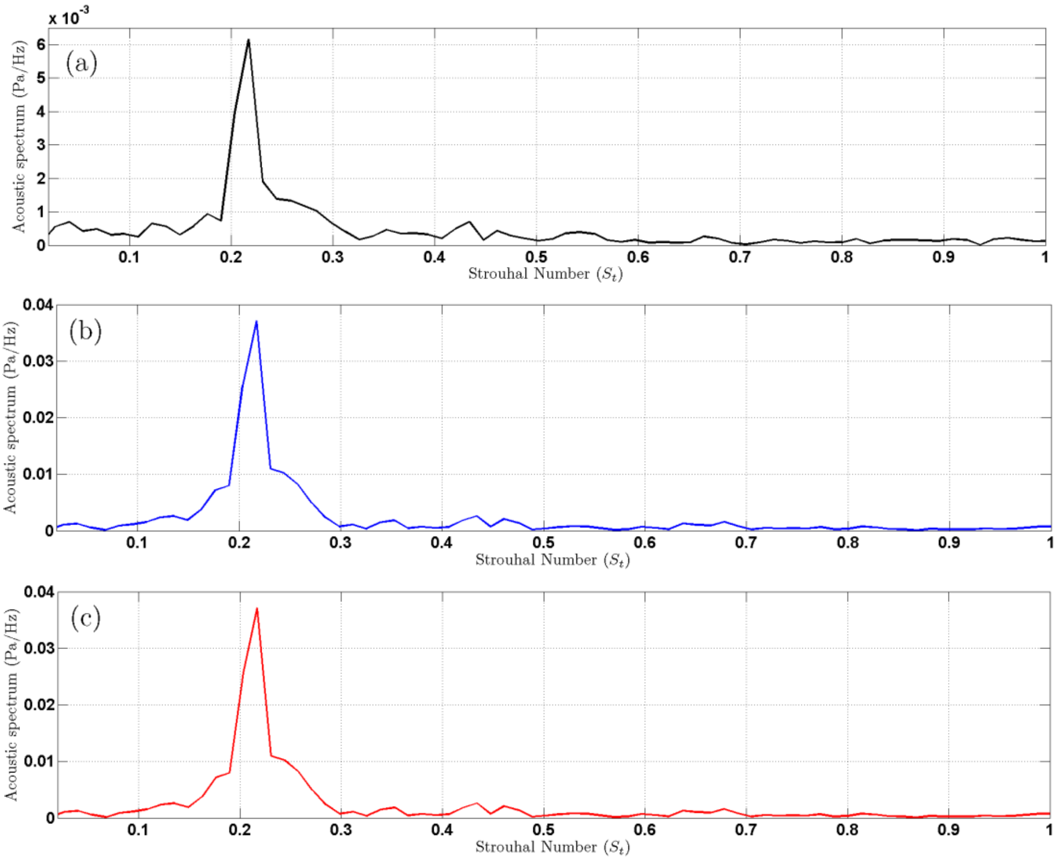

Figure 3. Far-field acoustic spectrum of the (a) direct, (b) scattered and (c) total acoustic pressure fields corresponding to the Welch segment 1 obtained numerically at the node $x = -0.177$ m, $y = -0.35$ m located on the bottom boundary

4. Aeroacoustic Time-Reversal (TR) Simulation

The TR simulation was implemented by numerically solving the two-dimensional LEE given by Eqs. (6-8) using the Pseudo-Characteristic Formulation (PCF) [14] in reverse time $\tilde{t}$ on a square-domain $|x| \le L_0$, $|y| \le L_0$ with anechoic boundary conditions and enforcing the synthesised time-reversed acoustic pressure history $\tilde{p}(x, y, \tilde{t})$ at all four boundaries [15].

$$\begin{aligned}
\frac{\partial \tilde{p}}{\partial \tilde{t}} &= -\frac{\rho_0 c_0}{2}\left(\left(\tilde{X}^{+}_{\text{linear}} + \tilde{X}^{-}_{\text{linear}}\right) + \left(\tilde{Y}^{+}_{\text{linear}} + \tilde{Y}^{-}_{\text{linear}}\right)\right) \\
\frac{\partial \tilde{u}}{\partial \tilde{t}} &= -\frac{1}{2}\left(\tilde{X}^{+}_{\text{linear}} - \tilde{X}^{-}_{\text{linear}}\right) - \tilde{v}\left(-\frac{\partial U_\infty}{\partial y}\right) - \left(\tilde{u} + \frac{-U_\infty}{c_0}\frac{\tilde{p}}{\rho_0 c_0}\right)\left(-\frac{\partial U_\infty}{\partial x}\right) \\
\frac{\partial \tilde{v}}{\partial \tilde{t}} &= -\frac{1}{2}\left(\tilde{Y}^{+}_{\text{linear}} - \tilde{Y}^{-}_{\text{linear}}\right) - \left(-U_\infty\right)\frac{\partial \tilde{v}}{\partial x}
\end{aligned} \tag{6-8}$$

where

$$\tilde{X}^{\pm}_{\text{linear}} = \pm\left(c_0 \mp U_\infty\right)\left(\frac{1}{\rho_0 c_0}\frac{\partial \tilde{p}}{\partial x} \pm \frac{\partial \tilde{u}}{\partial x}\right) \tag{9}$$

$$\tilde{Y}^{\pm}_{\text{linear}} = \pm\, c_0\left(\frac{1}{\rho_0 c_0}\frac{\partial \tilde{p}}{\partial y} \pm \frac{\partial \tilde{v}}{\partial y}\right) \tag{10}$$

denote a pair of opposing fluxes propagating towards the x and y directions, respectively [2]. Furthermore, $\tilde{u}$ and $\tilde{v}$ denote acoustic velocities $(\text{m} \cdot \text{s}^{-1})$ along the x and y directions, respectively, whilst the free-stream velocity U_∞ is set to zero during TR simulation. The spatial derivative of acoustic pressure and velocities in the opposing fluxes $\left(\tilde{X}^{\pm}_{\text{linear}},\ \tilde{Y}^{\pm}_{\text{linear}}\right)$ of the PCF were computed using an overall upwind-biased Finite-Difference (FD) scheme that is formulated using a fourth-order, seven-point optimized upwind-biased FD scheme [16] at interior nodes and a seven-point optimised backward FD scheme at the boundary nodes [17]. The third-order Total-Variation-Diminishing Runge-Kutta scheme was used for time-integration [13] and as indicated earlier, the $CFL = 0.2$. The instantaneous time-reversed acoustic pressure field $\tilde{p}\left(x, y, \tilde{t}\right)$ during the TR simulations was obtained using the superposition technique [2].

The TR simulation was implemented over the reverse time interval $\tilde{t} = \left[0,\ N_{\max}\Delta t = 10000\Delta t\right]$ whereby the aeroacoustic source location/characteristics were obtained by determining the focal spots in the RMS time-reversed acoustic pressure field (computed when a steady-state acoustic field is observed throughout the domain) denoted by $\tilde{p}^{TR}_{RMS}\left(x, y\right)$. The focal spot maximum is termed the focal point. The $\tilde{p}^{TR}_{RMS}\left(x, y\right)$ field was converted to the dB scale (*w.r.t.* $p_{ref} = 2\times10^{-5}$ Pa) and is denoted by $\tilde{p}^{TR}_{\text{dB}}\left(x, y\right)$, see Mimani *et al*. [15].

5. Results and Discussion

The TR source maps were obtained using the time-reversed acoustic pressure history at the four line arrays synthesised from the far-field spectrum of the direct, scattered and total acoustic pressure field corresponding to Welch segment 1 and 2, respectively, over a square domain $|x| \leq 0.3$ m, $|y| \leq 0.3$ m. However, it was observed for each of the three cases, the magnitude of the RMS field at the focal spots, the side-lobes/spurious maxima regions as well as their respective size vary significantly over the two Welch segments. Therefore, an average of the source maps corresponding to the Welch segments 1 and 2 was computed for each case.

Figure 4(a)-(c) shows the average TR source maps due to the direct acoustic field, scattered acoustic field and the total acoustic field, respectively. It is noted that in Figs. 4(a)-(c), the cylinder is denoted by a circle **O** and is located at the origin whilst the colourbar indicates the magnitude of the RMS acoustic pressure field in dB.

The pattern of formation of four focal spots located in proximity in Fig. 4(a) signifies a lateral quadrupole nature [2, 15] of the flow-induced source generated in the wake of the cylinder due to the direct acoustic radiation at the Aeolian tone although the formation of side-lobes of magnitude comparable to that of the focal spots as well as the occurrence of spurious maxima region near the top-right and bottom-right corners of the domain makes it somewhat difficult to readily identify the source nature. Nevertheless, these results demonstrate the validity of the hybrid CFD-BEM technique coupled with the TR method for characterising the lateral quadrupole nature generated by the direct acoustic radiation at the Aeolian tone which is consistent with previous studies [18]. The geometrical centre of the four focal spots is taken as the predicted source location and is denoted by a cross **X**. This symbolic convention for the predicted source location is also followed in the other source maps.

Figure 4(b) exhibits two focal spots that are located in proximity, thereby signifying a lift-dipole nature of the flow-induced source at the Aeolian tone frequency [12] generated near the cylinder-axis due to scattering of the direct acoustic field by the cylinder. The geometrical centre of the two focal spots is taken as the predicted dipole location and is denoted by a cross **X**. However, it is noted that the formation of side-lobes and the occurrence of spurious maxima region near the boundaries (similar to Figs. 4(a)) makes it somewhat difficult to readily identify the lift-dipole nature. Nonetheless, this source map again demonstrates the success of the novel technique for characterising the lift-dipole nature generated at the Aeolian tone due to the scattered field which is in agreement with previous studies [12].

Figure 4(c) is observed to be qualitatively similar to Fig. 4(b); the lift-dipole source nature generated due to the total acoustic pressure field can be easily identified by the two focal spots located in proximity. This is consistent with the classical result that a lift-dipole source nature is expected at the Aeolian tone (or vortex-shedding frequency) of a cylinder located in cross-flow using far-field experimental data wherein only the total acoustic pressure field can be recorded [12].

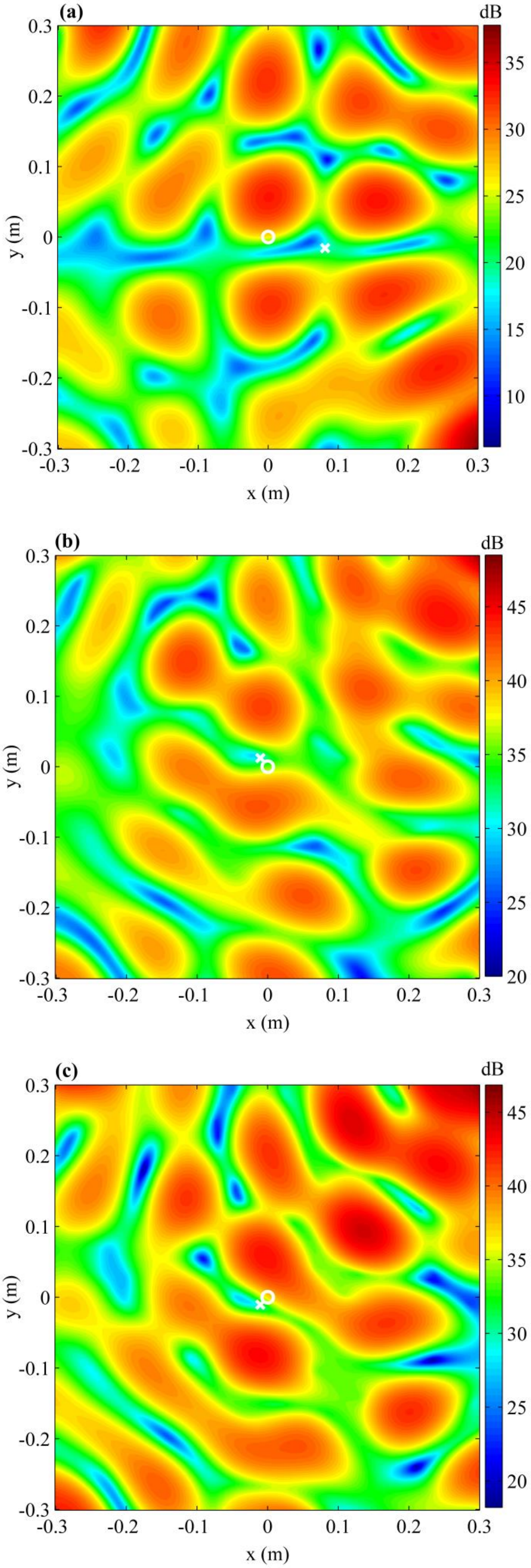

Figure 4. Average TR source maps due to (a) direct, (b) scattered and (c) total acoustic pressure fields

6. Conclusions

This paper has presented a simulation-based approach using the hybrid CFD-BEM and aeroacoustic TR simulations for characterising the nature of flow-induced noise sources. The validity of this approach was demonstrated on a benchmark problem of flow-induced noise generated at the Aeolian tone due to a cylinder located in a low Mach number flow. The hybrid CFD-BEM method was used to compute the far-field acoustic spectral data at the boundaries for the direct, scattered and total field whereby the acoustic pressure time-history was synthesised by assuming a purely sinusoidal signal corresponding to the Aeolian tone frequency that was enforced at the boundary nodes during aeroacoustic TR simulations. It was shown that the TR source maps indicate a lateral quadrupole source nature due to the direct acoustic field whilst a lift-dipole nature was indicated due to the scattered and the total acoustic fields. These TR results are supported by published literature on Aeolian tonal noise, thereby demonstrating the validity of novel technique proposed here.

References

[1] Porteous, R., Prime, Z., Doolan, C. J., Moreau, D.J. and Valeau, V. “Three-dimensional beamforming of dipolar aeroacoustic sources”, *Journal of Sound and Vibration*, **355**, 117-134, (2015).

[2] Mimani, A., Prime, Z., Doolan, C. J. and Medwell, P.R. “A sponge-layer damping technique for aeroacoustic time-reversal”, *Journal of Sound and Vibration*, **342**, 124-151 (2015).

[3] Norberg, C. “Fluctuating lift on a circular cylinder: Review and new measurements”, *Journal of Fluids and Structures*, **17**, 57-96, (2003).

[4] Croaker, P., Kessissoglou, N. and Marburg, S. “Strongly singular and hypersingular integrals for aeroacoustic incident fields”, *International Journal for Numerical Methods in Fluids*, **77**, 274-318, (2015).

[5] Lighthill, M.J. “On sound generated aerodynamically, I. General theory”, *Proceedings of the Royal Society A*, **211**, 564-587, (1952).

[6] Burton, A.J. and Miller, G.F. “The application of integral equation methods to the numerical solution of some exterior boundary-value problems”, *Proceedings of the Royal Society of London. Series A, Mathematical and Physical Sciences*, **323**, 201-210, (1971).

[7] Weller, H.G., Tabor, G., Jasak, H. and Fureby, C. “A tensorial approach to computational continuum mechanics using object-oriented techniques”, *Computer in Physics*, **12**, 620-631, (1998).

[8] Kirkup, S.M. *The Boundary Element Method in Acoustics*, Integrated Sound Software, 1998.

[9] Seo, J. and Moon, Y. “Aerodynamic noise prediction for long-span bodies”, *Journal of Sound and Vibration*, **306**, 564-579, (2007).

[10] Szepessy, S. and Bearman, P. W. “Aspect ratio and end plate effects on vortex shedding from a circular cylinder”, *Journal of Fluid Mechanics*, **234**, 191-217, (1992).

[11] Jacob, M.C., Boudet, D., Casalino, D. and Michard, M. “A rod-airfoil experiment as a benchmark for broadband noise modelling”, *Theoretical and Computational Fluid Dynamics*, **19**, 171-196, (2005).

[12] Mimani, A., Moreau, D.J., Prime, Z. and Doolan, C.J. “Enhanced focal-resolution of dipole sources using aeroacoustic time-reversal in a wind tunnel”, *Mechanical Systems and Signal Processing*, accepted for publication on the 27th September 2015.

[13] Gottlieb, S. and Shu, C.-W. “Total variation diminishing Runge-Kutta schemes”, *Mathematics of Computation*, **67**, 73-85, (1998).

[14] Sesterhenn, J. “A characteristic-type formulation of the Navier-Stokes equations for high order upwind schemes”, *Computers and Fluids*, **30**, 37-67, (2000).

[15] Mimani, A., Doolan, C.J. and Medwell, P.R., “Multiple line arrays for the characterization of aeroacoustic sources using a time-reversal method”, *Journal of the Acoustical Society of America*, **134**, EL327-EL333 (2013).

[16] Zhuang, M. and Chen, R.F. “Applications of high-order optimized upwind schemes for computational aeroacoustics”, *AIAA Journal*, **40**, 443-449, (2002).

[17] Tam, C.K.W. “Computational aeroacoustics: Issues and methods”, *AIAA Journal*, **33**, 1788-1796, (1995).

[18] Khalighi, Y. *Computational aeroacoustics of complex flows at low Mach number*, PhD Thesis, Stanford University, 2010.